RSC Advances

PAPER

View Article Online
View Journal | View Issue

Cite this: *RSC Adv.*, 2018, **8**, 32003

Discovering a new MgH_2 metastable phase†

Mohamed Sherif El-Eskandarany,* Mohammad Banyan and Fahad Al-Ajmi

Received 23rd August 2018
Accepted 10th September 2018

DOI: 10.1039/c8ra07068g

rsc.li/rsc-advances

Formation of a new metastable fcc-MgH_2 nanocrystalline phase upon mechanically-induced plastic deformation of MgH_2 powders is reported. Our results have shown that cold rolling of mechanically reacted MgH_2 powders for 200 passes introduced severe plastic deformation of the powders and led to formation of micro-lathes consisting of γ- and β-MgH_2 phases. The cold rolled powders were subjected to different types of defects, exemplified by dislocations, stacking faults, and twinning upon high-energy ball milling. Long term ball milling (50 hours) destabilized β-MgH_2 (the most stable phase) and γ-MgH_2 (the metastable phase), leading to the formation of a new phase of face centered cubic structure (fcc). The lattice parameter of fcc-MgH_2 phase was calculated and found to be 0.4436 nm. This discovered phase possessed high hydrogen storage capacity (6.6 wt%) and revealed excellent desorption kinetics (7 min) at 275 °C. We also demonstrated a cyclic-phase-transformation conducted between these three phases upon changing the ball milling time to 200 hours.

The worldwide interest in MgH_2 is attributed to the natural abundance of Mg metal, and its capability to store hydrogen up to 7.60 wt% (0.11 kg H_2 L^{-1}).[1–3] Among the metal hydride family, MgH_2 has been considered as a promising candidate for solid-state hydrogen storage.[4–6] Despite the attractive properties of MgH_2, and the simplicity for producing the compound on an industrial scale at ambient temperature *via* a reactive ball milling (RBM) technique,[7,8] MgH_2 is a very stable compound, and possesses slow kinetics of hydrogenation and dehydrogenation under 300 °C.[9] Since the 1990s efforts have been made in order to destabilize MgH_2 and improve its hydrogenation and dehydrogenation kinetics upon doping with a long list of catalysts.[10–15] Most of the used catalysts showed significant enhancement of the kinetics behavior for MgH_2, indexed by a decreasing decomposition temperature and a speed-up of its kinetics behavior.[16–20] In spite of the beneficial effects obtained upon adding such foreign catalytic agents, they always lead to a dramatic decrease of the hydrogen storage capacity of MgH_2.[21,22]

Apart from doping MgH_2 powders with catalysts, it has been experimentally demonstrated by some authors that changing the crystal structure of stable β-tetragonal MgH_2 phase to a less stable phase of γ-orthorhombic MgH_2 led to improve the gas uptake/release kinetics and decrease the hydrogenation temperature without drastic decreasing of the storage capacity.[23–26] The β-to-γ phase transformations can be attained *via* severe plastic deformation (SPD)[27] at ambient temperature by different approaches such as high-energy ball milling (HEBM),[28] cold rolling (CRing),[29] equal channel angular pressing (ECAP),[30] and high pressure torsion (HPT).[22,31] A common result of these employed techniques is the formation of nanocrystalline phase along with introducing high intensity defects, leading to increase of grain boundaries density. Presence of these defects in the lattice leads to create nucleation points for hydrogenation, where existence of large number of grain boundaries assists fast diffusion pathways for hydrogen.

The present work has been addressed in part to study the effect of HEBM on the structure and decomposition properties of CRed MgH_2 powders. Moreover, we aimed to investigate experimentally the possibility of formation a new metastable MgH_2 phase rather than the reported g-phase and theoretically calculated δ and ε phases[32] upon long term of milling.

For the purpose of the present study, 5 g Mg (~80 μm, 99.8 wt%) powder was balanced inside a He gas atmosphere-glove box and sealed together with fifty hardened steel-balls (11 mm in diameter), using ball-to-powder weight ratio as 40 : 1. The vial was then evacuated to the level of 10^{-3} bar and then filled with 50 bar of H_2. The RBM process was carried out at room temperature, using planetary-type HEBM. After 25 hours (h) of RBM, the vial was open inside the glove box to discharge the powders. The powders were charged and sealed in a stainless steel (SUS304) tube (0.8 cm diameter and 20 cm length) inside the glove box. The tube contained MgH_2 powders were severely CRed for different number of passes (1 to 200 passes), using two-drum type manual cold roller (11 cm wide × 5.5 cm rollers diameter). The as-CRed powders for 200 passes were then HEBMed under hydrogen gas for different milling time, in the range between 3 h to 50 h. All the samples were characterized by means of X-ray diffraction (XRD) with Cu radiation,

Nanotechnology and Advanced Materials Program, Energy and Building Research Center, Kuwait Institute for Scientific Research, Safat 13109, Kuwait. E-mail: msherif@kisr.edu.kw

† Electronic supplementary information (ESI) available. See DOI: 10.1039/c8ra07068g

field-emission high-resolution transmission electron microscope (FE-HRTEM) equipped with energy-dispersive X-ray spectroscopy (EDS), field emission scanning electron microscope (FE-SEM)/EDS, and differential scanning calorimeter (DSC). The absorption/desorption kinetics were investigated *via* Sievert's method in different temperatures under hydrogen gas pressure in the range between 200 mbar to 8 bar.

The XRD patterns of MgH_2 powders obtained after 25 h of RBM is shown in Fig. 1a. Bragg peaks corresponding to starting hcp-Mg powders were hardly seen and replaced by sharp diffracted lines related to γ- and β-MgH_2 phases, as elucidated in Fig. 1a. The SEM observations indicated the powders tendency to agglomerate, forming large aggregates upon CRing for 25 passes (Fig. 2a). Increasing the CRing passes to 200 times led to grain refinement, as implied by the broadening in the Bragg-peaks presented in Fig. 1b. At this stage, micro-bands with thickness of 143 μm were developed as a result of cold working generated during CRing process, as shown in Fig. 2b. The FE-HRTEM image of as-CRed powders for 200 passes indicated the development of lattice imperfections (*e.g.* stacking faults and deformation twins). This is implying the mechanically-induced SPD, as elucidated in ESI, Fig. S1.†

In order to study the effect of HEBM on the stability of cold-rolled MgH_2 aggregates, the powders were charged into tool steel vial and ball milled under 50 bar of H_2 for different milling time. The XRD pattern of CRed MgH_2 powders obtained after 200 CR passes and then HEBMed for 50 h is displayed in Fig. 1c. Obviously, the Bragg peaks corresponding to γ- and β-MgH_2 phases were completely vanished and replaced by new Bragg peaks of unreported phase, appeared at scattering angles (2θ) of, 35.034, 40.584, 58.758, 70.115, and 73.868 (Fig. 1c). XRD analysis indicated that this discovered MgH_2 phase has face centered cubic structure (fcc) of space group, $Fm\bar{3}m(225)$. The lattice parameter (a_o) of this phase, calculated from (111) was

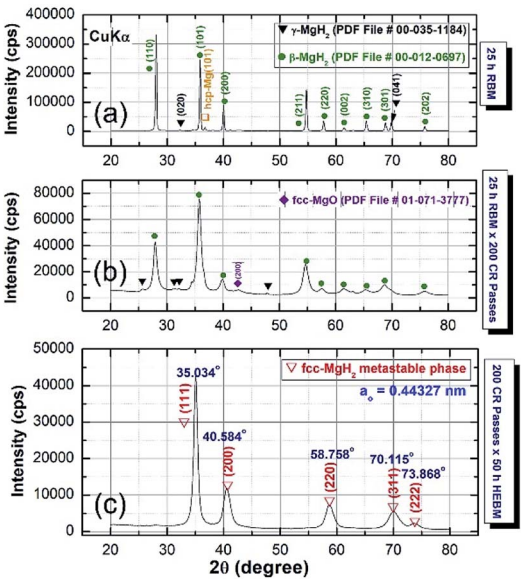

Fig. 1 XRD patterns of MgH_2 powders obtained after 25 h of RBMing (a), and then CRed for 200 passes (b). XRD pattern of CRed powders for 200 passes and then HEBMEd for 50 h is presented in (c).

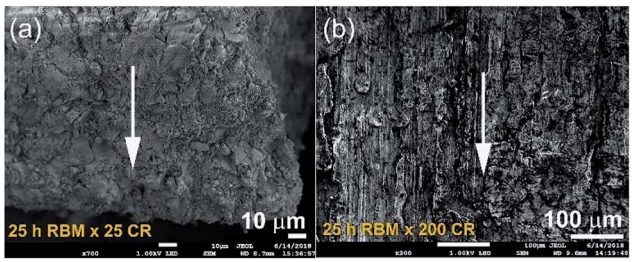

Fig. 2 FE-SEM micrographs taken at accelerated voltage of 1 kV of MgH_2 powders obtained after 25 h of RBMing and then CRed for (a) 25, and (b) 200 passes.

0.44361 nm. The as-synthesized fcc-MgH_2 powders had fine spherical particles with sizes distributed in the range between 0.25 μm to 1 μm, as displayed in Fig. 3.

Table 1 presents some of structural parameters related to this new phase, indexed by the interplanar spacing for the corresponding Miller indexes (h,k,l) and 2θ.

The FE-HRTEM image of the as-CRed powders for 200 passes and then HEBMed for 50 h is shown in Fig. 4. The image revealed Moiré fringe image for 3 intimated nanograins. Filtered-fringe images corresponding to Zone I is presented in Fig. 4a. The d-spacing related to fcc-MgH_2 (111) was calculated and found to be 0.2559 nm, where the corresponding a_o was calculated and found to be 0.4433 nm. These values matches well with the XRD analysis (Table 1). The FFT image, which is displayed in Fig. 4c, was taken from Zone I and oriented to [001] axis, where the corresponding FFT showed spot-electron diffraction pattern related to fcc-MgH_2 (111).

Fig. 5 presents DSC thermograms of MgH_2 powders obtained after 25 h of RBM, consequently cold-rolled for 200 passes and then HEBM for different times, as indexed in Fig. 5. The DSC curves for the powders obtained after 25 h of RBM and then cold-rolled only without milling for different passes are shown together in ESI (Fig. S2†).

The decomposition temperature of the powders obtained after 25 h of RBM (before applying CRing process) was 415 °C (Fig. S2†), and tended to decrease sharply to 361 °C upon powders CRing for 200 passes, as displayed in Fig. S2.† This significant decreasing on the decomposition temperature upon increasing the number of

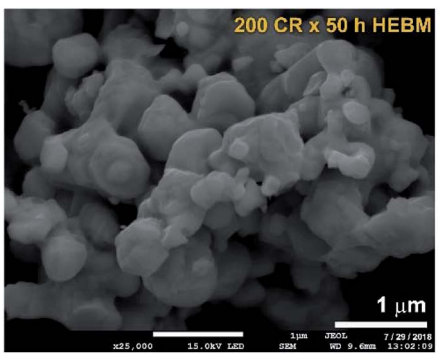

Fig. 3 FE-SEM micrograph of MgH_2 powders obtained after 25 h of RBM, CRed for 200 passes and finally HEBMed for 50 h.

Table 1 Unit cell characteristics of discovered fcc-MgH_2 phase prepared in the present work. The lattice parameter for each Miller indexes was calculated based on Bragg equation, using X-ray wavelength (λ) of Cu radiation (0.15418 nm)

Peak position, 2θ (degree)	Interplanar spacing, d (nm)	Miller indexes (h,k,l)	Lattice parameter, a_o (nm)
35.034	0.25612	111	0.44361
40.584	0.22229	200	0.44458
58.758	0.15713	220	0.44443
70.115	0.13421	311	0.44512
73.868	0.12829	222	0.44441

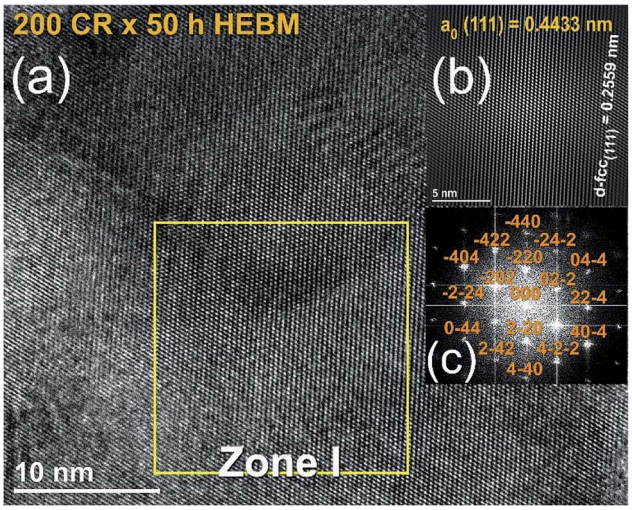

Fig. 4 (a) FE-HRTEM image, (b) filtered atomic resolution image of Zone I, and (c) FFT image of MgH_2 powders obtained after 25 h of RBM, consequently CRed for 200 passes and finally HEBMed for 50 h.

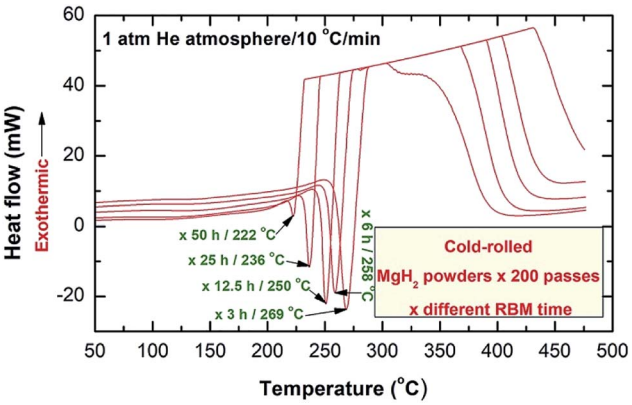

Fig. 5 DSC thermograms of MgH_2 powders obtained after 25 h of RBM, consequently CRed for 200 passes and final HEBMed for different milling times (6 h to 50 h). The values related to the peak temperatures for each milling time is elucidated in each curve.

CRing passes was attributed to destabilization of MgH_2, yielded from introducing severe plastic deformation to the powders.

The XRD pattern for MgH_2 powders obtained after 200 CRing passes and then heated in DSC up to 500 °C showed the presence of a single hcp-Mg phase (Fig. S3†). The as-HEBMed of the powders CRed for 200 passes revealed single endothermic events related to the decomposition reaction (Fig. 5).

Obviously, the peak temperature of the samples obtained after different milling times shifted monotonically to the low temperature side with increasing the HEBMing time (Fig. 5). After 50 h of milling (single metastable fcc-MgH_2 phase), the decomposition temperature was reordered to be 222 °C (Fig. 5). This temperature was far below the corresponding decomposition temperature (361 °C, Fig. S3†) corresponding to as-CRed powders (γ- + β-MgH_2 phases) obtained after 200 passes (Fig. S3†).

The powders obtained after 50 h of HEBM was annealed in the DSC at 220 °C (just beyond decomposition onset temperature) and at 375 °C (well above the onset decomposition temperature) for 7 min. XRD pattern of the first sample annealed at 220 °C indicated metastable fcc-MgH_2-to-stable β-MgH_2 phase transformation, as implied by disappearance of fcc-Bragg peaks and the presence of pronounced sharp Bragg lines corresponding to β-MgH_2 coexisted with small volume fraction of γ-MgH_2 (Fig. 6a).

FE-HRTEM (Fig. 7a) and NBD (Fig. 7b) analysis of the annealed sample at 220 °C confirmed the presence of γ- and β-MgH_2 phases and a complete disappearance of metastable fcc-MgH_2, as displayed in Fig. 7a and b, respectively. In contrast, XRD pattern of the sample annealed at 375 °C showed the Bragg peaks of hcp-Mg coexisted with small volume fraction of undecomposed β-MgH_2 crystals (Fig. 6b). It can be concluded from the structural and thermal analysis that γ- and β-MgH_2 phases tended to transform to a new metastable phase upon

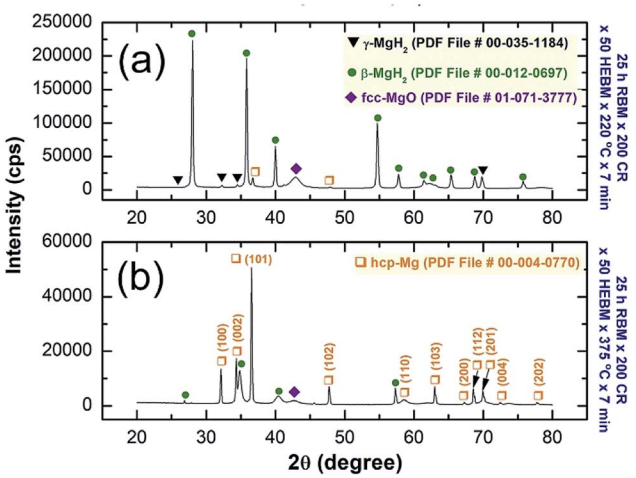

Fig. 6 XRD patterns of the samples obtained after 50 h and then annealed in the DSC for 7 min at (a) 220 °C, and (b) 375 °C for 7 min.

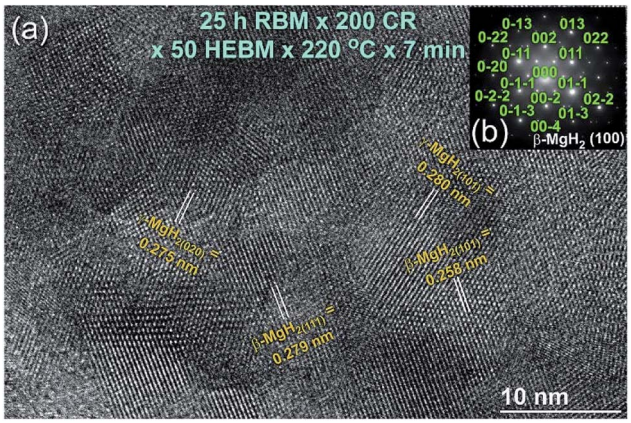

Fig. 7 (a) FE-HRTEM, and (b) NBDP of the sample milled for 50 h and then annealed in the DSC at 220 °C for 7 min.

CRing for 200 passes followed by HEBMing for 50 h. The obtained metastable fcc-MgH_2 phase transformed into more stable phases of γ- and β-MgH_2 phases when annealed at 220 °C for 7 min. A complete phase transformation to hcp-Mg was attained upon annealing fcc-MgH_2 at 375 °C.

Further experiments were conducted to examine the stability of fcc-MgH_2 phase against the mechanical deformation generated by HEBMing. The powders obtained after 50 h were continuously milled for 100 h, 150 h, and 200 h. The XRD pattern of the milled powders for 100 h indicated the disappearance of Bragg peaks related fcc-MgH_2 phase, which were replaced by diffracted lines related to γ- and β-MgH_2 phases as shown in Fig. 8a. This implies the disability of fcc-MgH_2 phase to withstand against the shear and impact forces generated by the milling media. Surprisingly, increasing the HEBMing to 150 h led to clear γ- , β-MgH_2 to fcc-MgH_2 (less stable phase) phase transformation (Fig. 8b). This is indicated by the presence of Bragg peaks related to fcc-MgH_2 phase and the disappearance of the diffracted lines corresponding to the MgH_2 phases, as displayed in Fig. 8b.

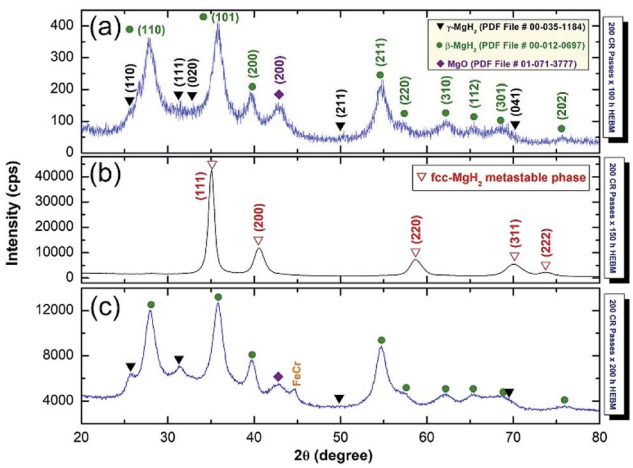

Fig. 8 XRD patterns of as-CRed MgH_2 powders for 200 passes and then HEBMed for (a) 100 h, (b) 150 h, and (c) 200 h.

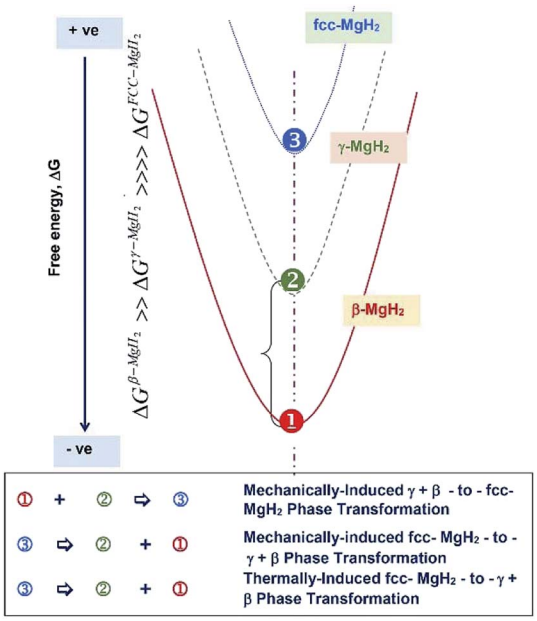

Fig. 9 Schematic presentation of free energy changes conducted upon HEBMing CRed MgH_2 powders for long term of milling.

Fig. 9 presents a schematic illustration of free energy changes of β-γ-fcc MgH_2 phases upon increasing HEBM time. Based on the results motivated of the present study, mechanically-induced fcc-MgH_2 to γ- and β-MgH_2 phase transformation (point 3-to-points 2 + 3) was achieved upon increasing the milling time to 100 h. Introducing severe lattice imperfections to the fcc-phase is proposed to be responsible to insist this metastable phase to gain free energy and hence transformed into a more stable phase, as illustrated in Fig. 9. This phase transformation can be taken place upon annealing the powders *via* thermally induced phase transformation, as indexed by point 3-to-points 2 + 1 (Fig. 9).

The obtained γ- and β-MgH_2 composite phases were subjected plastic deformation and defects, leading to lose free energy and transformed to the same metastable fcc-MgH_2 phase with further milling time (150 h), as denoted by points 1 + 2 to point 3 (Fig. 9). Further increasing the milling time (200 h) led fcc-MgH_2 to gain energy and failed into more stable phases of γ- and β-MgH_2.

Since high-energy ball milling process introduces intensive vacancies, lattice defects, grain boundaries and surfaces, the ball-milled powders can store a large amount of mechanical-strain energy.[33,34] Introducing such defects to the crystalline lattice destroys the periodical structure of the stable tetragonal-MgH_2 phase, leading to the formation of a less stable phase (fcc-MgH_2). Moreover, the present result suggests that the formation enthalpy of the metastable fcc-MgH_2 phase is comparable to the γ- and β-MgH_2 phases and the energy barrier between these three phases is probably rather low to allow such cyclic-phase transformations. We should emphases that all the results obtained from XRD analysis were used to determine the weight percentage of each phase, using the approaches described by Guan *et al.*,[35] Ma *et al.*,[36] Yu *et al.*,[37] and Cheng *et al.*[38]

Fig. 10 displays the dehydrogenation kinetics behaviors of the CRed powder obtained after 200 passes and then HEBMed for 50 h (fcc-MgH_2 phase). The measurements were conducted in the temperature range of 175 °C to 275 °C under 200 mbar.

In order to maintain the crystal structure of the powders (fcc-MgH_2 phase) obtained after this stage of milling, the desorption kinetics measurements measured without activation for 5 individual samples (Fig. 10a). All samples were successfully desorbed their hydrogen storage with different time scale. Generally, the fcc-MgH_2 powders showed advanced dehydrogenation characteristics over γ- and β-MgH_2 phases. At 175 °C, the sample desorbed ~4 wt% H_2 within 40 min (Fig. 10a). However, the powders desorbed about 6.5 wt% H_2 within 22 min at 200 °C (Fig. 6a). Increasing the applied temperature to 225 °C and 250 °C, improved the dehydrogenation kinetics of fcc-MgH_2, indicated by the short time required to desorb 6.6 wt% H_2 in 17 min and 10 min, respectively (Fig. 10a).

Outstanding desorption kinetics was conducted at 275 °C, when the sample desorbed 6.6 wt% H_2 within 7 min, as elucidated in Fig. 10a. We should emphases that the XRD patterns for the examined samples at temperature range laid between 175 °C to 225 °C revealed presence of Bragg peaks corresponding to γ- and β-MgH_2 phases. However, the XRD pattern for those samples examined at higher temperatures (250 °C and 275 °C) revealed diffracted lines of hcp-Mg phase.

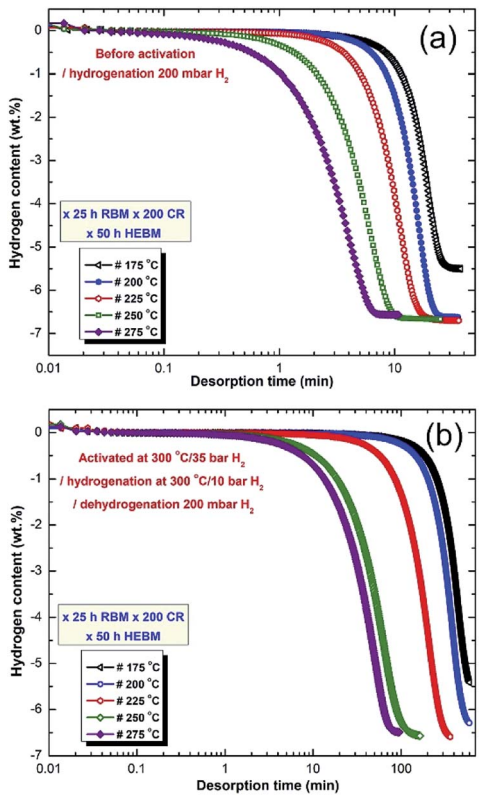

Fig. 10 Dehydrogenation kinetics measured for 10 individual samples of MgH_2 powders obtained after 25 h of RBM, consequently CRed for 200 passes and then HEBMed for 50 h. The measurements were conducted under 200 mbar H_2 (a) without powders activation, and (b) after activated the powders at 300 °C under 10 bar H_2.

Fig. 10b displays the dehydrogenation kinetics conducted for the same samples shown in 10a, however, they were activated firstly at 300 °C (far above the transformation temperature of fcc-MgH_2 to γ- and β-MgH_2 phases) under 25 bar H_2. Based on this activation step condition, all the samples lost their fcc-structure and completely transformed into γ- and β-MgH_2 phases. This led to a significant deduction of dehydrogenation kinetics that become very slow when compared with the same samples shown in Fig. 10a. For example, the sample examined at 175 °C required more than 650 min to desorb less than 5.5 wt% H_2 (Fig. 10b). The two samples examined at 200 °C and 225 °C desorbed about 6.4 and 6.6 wt% H_2 within 600 and 390 min, respectively (Fig. 10b). Comparing the necessary desorption time (100 min) for the sample examined at 275 °C to release 6.6 wt% H_2 (Fig. 10b) with that time required (7 min) for fcc-MgH_2 sample (Fig. 10a) to desorb same hydrogen amount at the same temperature, we can realize that the kinetics desorption of fcc-MgH_2 phase is 14 time faster than γ- and β-MgH_2 phases.

Conclusions

In summary, we have successfully developed a new metastable phase of fcc-MgH_2 ($Fm\bar{3}m$(225)), which its lattice parameter (a_o) was calculated and found to be 0.4436 nm. This discovered phase was obtained upon cold rolling of reacted ball milled MgH_2 powders for 200 passes and consequently high energy ball milled for 50 h. The results have shown outstanding desorption kinetics of this new phase, indexed by its capability to desorb 4–6.6 wt% H_2 at relatively low temperature (175 °C to 250 °C) in short time. At 275 °C, metastable fcc-MgH_2 completely discharged 6.6 wt% H_2 within 7 min. This metastable phase transformed completely into γ- and β-MgH_2 upon annealing at 220 °C for 7 min. Moreover, the present study confirms that mechanically induced fcc-MgH_2 to γ- and β-MgH_2 phase transformation can be cyclically achieved upon increasing the high-energy ball milling time.

Conflicts of interest

There are no conflicts to declare.

Acknowledgements

Appreciation is extended to the Kuwait Foundation for the Advancement of Sciences (KFAS) for the partial financial support of this study related to the Project EA061C under a contract number: P315-35EC-01. The financial support received by the Kuwait Government through the Kuwait Institute for Scientific Research for purchasing the equipment used in the present work, using the budget dedicated for the project (P-KISR-06-04) led by the first author of Establishing Nanotechnology Center in KISR is highly appreciated.

Notes and references

1 M. Jefferson, *Renewable Energy*, 2006, **31**, 571–582.

2 T. Yamada, J. Yin and K. Tanaka, *Mater. Trans.*, 2001, **42**, 2415–2421.
3 I. P. Jain, C. Lal and A. Jain, *Int. J. Hydrogen Energy*, 2010, **35**, 1121–1140.
4 L. Schlapbach and A. Züttel, *Nature*, 2001, **414**, 353–358.
5 B. Sakintuna, F. Lamari-Darkrim and M. Hirscher, *Int. J. Hydrogen Energy*, 2007, **32**, 1121–1140.
6 I. P. Jain, P. Jain and A. Jain, *Int. J. Hydrogen Energy*, 2010, **35**, 5133–5144.
7 A. Calka, *Appl. Phys. Lett.*, 1991, **59**, 1568–1570.
8 M. Sherif El-Eskandarany, K. Sumiyama, K. Aoki and K. Suzuki, *Mater. Sci. Forum*, 1992, **88**, 801–808.
9 G. Principi, F. Agresti, A. Maddalena and R. S. Lo, *Int. J. Hydrogen Energy*, 2009, **34**, 2087–2091.
10 G. Liang, J. Huot, S. Boily, A. Van Neste and R. Schulz, *J. Alloys Compd.*, 1999, **292**, 247–252.
11 N. A. Ali, et al., *RSC Adv.*, 2018, **8**, 15667–15674.
12 A. Bhatnagar, *et al.*, *J. Mater. Chem. A*, 2016, **4**, 14761–14772.
13 Y. Wang, *et al.*, *J. Mater. Chem. A*, 2014, **2**, 16285–16291.
14 M. Sherif El-Eskandarany, *Sci. Rep.*, 2016, **6**, 26936, DOI: 10.1038/srep26936.
15 M. Sherif El-Eskandarany, *et al.*, *Mater. Chem. Phys.*, 2018, **203**, 17–26.
16 H. Liu, X. Wang, Y. Liu, Z. Dong, G. Cao, S. Li and M. Yan, *J. Mater. Chem. A*, 2013, **1**, 12527–12535.
17 J. Huot and J. Dufour, *J. Alloys Compd.*, 2007, **446–447**, 147–151.
18 M. S. El-Eskandarany, H. Al-Matrouk, E. Shaban and A. Al-Duweesh, *Int. J. Hydrogen Energy*, 2015, **40**, 10139–10149.
19 J. Chen, H. Fu, Y. Xiong, J. Xu, J. Zheng and X. Li, *Nano Energy*, 2014, **10**, 337–343.
20 M. S. El-Eskandarany, H. Al-Matrouk, E. Shaban and A. Al-Duweesh, *Energy*, 2015, **91**, 274–282.
21 G. Liu, *et al.*, *Nanoscale*, 2013, **5**, 1074–1081.
22 K. Edalati, *et al.*, *Scr. Mater.*, 2018, **157**, 54–57.
23 C. Shen and K.-F. Aguey-Zinsou, *J. Mater. Chem. A*, 2017, **5**, 8644–8652.
24 X. Xiao, Z. Liu, S. Saremi-Yarahmadi and D. H. Gregory, *Phys. Chem. Chem. Phys.*, 2016, **18**, 10492–10498.
25 F. Cuevas, D. Korablov and M. Latroche, *Phys. Chem. Chem. Phys.*, 2012, **14**, 1200–1211.
26 Z. Wang, *et al.*, *J. Mater. Chem. A*, 2018, **6**, 5652–5660.
27 R. Z. Valiev, R. K. Islamgaliev and I. V. Alexandrov, *Prog. Mater. Sci.*, 2000, **45**, 103–189.
28 M. Sherif El-Eskandarany, E. Shaban and B. Al-Halaili, *Int. J. Hydrogen Energy*, 2014, **39**, 12727–12740.
29 S. Amira and J. Huot, *J. Alloys Compd.*, 2012, **520**, 287–294.
30 A. M. Jorge Jr, *et al.*, *Int. J. Hydrogen Energy*, 2014, **39**, 3810–3821.
31 Y. Mine, T. Tsumagari and Z. Horita, *Scr. Mater.*, 2010, **63**, 552–555.
32 P. Vajeeston, P. Ravindran, A. Kjekshus and H. Fjellvåg, *Phys. Rev. Lett.*, 2002, **89**, 175506–175509.
33 M. Sherif El-Eskandarany, K. Aoki, K. Sumiyama and K. Suzuki, *Acta Mater.*, 2002, **50**, 1113–1123.
34 M. Sherif El-Eskandarany and A. Inoue, *Phys. Rev. B*, 2007, **75**, 224109.
35 S. Guan, X. Fu, Y. Zhang and Z. Peng, *Chem. Sci.*, 2018, **9**, 1574–1585.
36 X. Ma, Q. Xiang, Y. Liao, T. Wen and H. Zhang, *Appl. Surf. Sci.*, 2018, **457**, 846–855.
37 J. Yu, W. Wang, B. Cheng and B.-L. Su, *J. Phys. Chem. C*, 2009, **113**, 6743–6750.
38 L. Cheng, Q. Xiang, Y. Liao and H. Zhang, *Energy Environ. Sci.*, 2018, **11**, 1362–1391.